Increasing Tracking Bandwidth for Deep-Space Optical Communications Using Linear Accelerometers

S. Lee,[1] G. G. Ortiz,[1] W. Liu,[1] and V. Garkanian[1]

In deep-space optical communications, acquisition, tracking, and pointing are all challenging because of the stringent—on the order of submicroradian—pointing requirement. To achieve this level of pointing accuracy, one must maintain high-bandwidth tracking control. Feasible tracking sources (beacons) include uplink laser beams and celestial objects such as the Earth, Moon, and stars. However, these tracking sources do not all provide the kilohertz tracking rate needed for pointing in deep space. One approach to enable a high tracking rate is to augment the tracking loop with inertial sensors to estimate high-frequency beacon movements. In this article, we discuss the use of linear accelerometers, mounted in a configuration to measure angular displacement, to achieve high-bandwidth tracking with dim beacon sources. The advantages of linear accelerometers (or angular accelerometers) are their low cost, high bandwidth, and small size compared with other inertial sensors such as gyros. Simulation and experimental results show good agreement. A tracking bandwidth increase of 11 times is demonstrated.

I. Introduction

High-data-rate, narrow-beam optical communication imposes the challenge of pointing a downlink beam to a fraction of the beam divergence, typically submicroradian in jitter and bias. This, in turn, requires a reference optical source, a beacon that can be used as a reference for closed-loop tracking/pointing control. In the past, acquisition, tracking, and pointing (ATP) system design required a beacon-tracking rate of several kilohertz to maintain the link properly. The required tracking rate depends on the platform vibration amplitude and frequency contents. A typical tracking source has been a laser beacon, especially for short-range optical communications such as intersatellite optical links [7].

However, the kilohertz beacon-tracking rate is not readily available in most deep-space applications due to the long range that limits beacon energy collected at the spacecraft telescope. This is true even for Earth-image-based tracking and star tracking [2]. The challenge is to achieve high-rate beacon

[1] Communications Systems and Research Section.

The research described in this publication was carried out by the Jet Propulsion Laboratory, California Institute of Technology, under a contract with the National Aeronautics and Space Administration.

tracking, even with low-rate beacon centroid measurements, that is, to estimate accurately the relative beacon position movements between the measured beacon centroids. In the past, similar problems were addressed with the use of inertial sensors: spacecraft attitude control using star trackers and gyros [4], and (in the case of the Hubble telescope) pointing using star trackers and various inertial sensors [8]. Although these applications are slightly different, the underlying principle is identical. Since the downlink target is moving very slowly in inertial space, all high-frequency motions come from the spacecraft. The high-frequency movements of the beacon relative to the target can be deduced from the measurements of the source (platform) vibrations that cause movements of the reference beacon (either laser beacon or celestial objects) on a charge-coupled device (CCD) array. If the error between the true and the estimated beacon positions is smaller than the error budget, a fast tracking rate can be maintained. Implementation of this concept requires accurate high-bandwidth inertial sensors. Among the possible inertial sensors are angular rate sensors, angle displacement sensors, gyros, and angular and linear accelerometers. Because of the low cost of linear accelerometers, as well as their accuracy over high bandwidth, small size, and availability, we chose to investigate their implementation in our research. This choice requires double integration for the position estimation from acceleration measurements. Furthermore, linear accelerometers are not as sensitive to low-frequency vibration as are gyros, a feature that limits their usage in the case of very low beacon intensity. However, previous use of linear accelerometers suggests their promise in a range of ATP applications. Linear accelerometers have been used successfully, for example, in the line-of-sight stabilization of a gimbaled imaging sensor suite [3] and in measuring the rotational and translational acceleration of a rigid body [1]. For deep-space optical communications, we sought to demonstrate that linear accelerometers could be used for beam pointing and control as well as for line-of-sight stabilization and for measuring the movement of a single body. For the double integration of accelerations to estimate displacements, some problems and solutions for zero-mean displacement signals have been addressed [5,6].

Having defined in this introduction the tracking and pointing problem to be addressed, we describe in the following how we estimated angular position using the triangular configuration of three accelerometers. Appendix A supplements this discussion by presenting the trapezoidal method of measuring linear displacements by means of a double integration of linear accelerations. For purposes of double integration, we needed to estimate initial platform linear velocity and to correct any potential acceleration bias due to misalignment of the accelerometers. For both operations, we used the least-squares method (described in Appendix B). We chose the least-squares approach primarily for ease of implementation, since we had not yet developed noise models for the platform. In the body of the article, we continue by describing the angular position estimation algorithm (APEA) that we devised, illustrated with a block diagram showing the major signal flows. In Appendix C, we provide an analysis of position estimation error. In the article proper, we continue by describing the baseline accelerometer configuration used for simulations. We then present the angular position estimates and corresponding errors resulting from both the ideal and measured accelerations. Finally, we summarize and discuss the performance of the APEA.

II. Beacon Position Estimation

The key issue in high-bandwidth tracking is the availability of beacon centroids at high rate. Given the limited beacon intensity in deep space (thus, small number of beacon centroids available) and the fact that the beacon movements are caused by spacecraft vibration, it is essential to be able to estimate the beacon centroids (or movements) at times when the beacon centroids are not available. In this section, we give the three-accelerometer configuration for the two angular position estimations and describe the algorithm used. Detailed treatments of the trapezoidal method for the linear displacement estimation, initial velocity/acceleration bias estimation, and random error analysis are given in the appendices.

A. Triangular Configuration of Three Linear Accelerometers

A pair of accelerometers (A_1 and A_2 in Fig. 1) can be used to estimate the angular displacement (or position with initial angular position) of the two-accelerometer body. The angle, θ, can be estimated

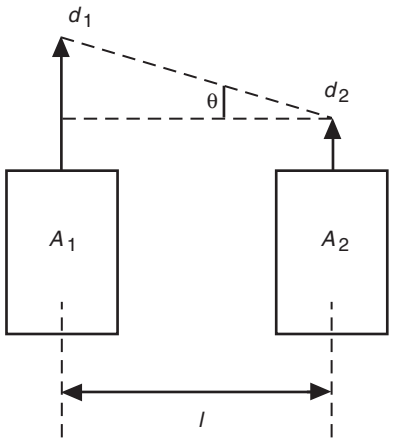

Fig. 1. A linear accelerometer arranged to estimate angular displacement.

from the individual readings of accelerometers, A_1 and A_2, after converting the accelerations into linear displacements, d_1 and d_2, with the small angle assumption:

$$\theta = \frac{d_1 - d_2}{l} \tag{1}$$

Since the separation, l, is a known measurable constant, θ is determined with the precision of the accelerometers. Linear displacement estimation from the acceleration measurements using the trapezoidal method is described in detail in Appendix A.

Angular displacements on two axis (α, β) can be obtained using three accelerometers, as shown in Fig. 2. Let α (horizontal) and β (vertical) be the angular displacements of the x–z plane around the z-axis and the y–z plane around the y-axis, respectively. A_1, A_2, and A_3 represent three accelerometers, and d_1, d_2, and d_3 represent the corresponding estimated linear displacements. Then, the two angular displacements due to the three linear displacements are

$$\left.\begin{aligned} \alpha &= \frac{d_1 - d_2}{l_1} \\ \beta &= \frac{\frac{d_1 + d_2}{2} - d_3}{l_2} \end{aligned}\right\} \tag{2}$$

where l_1 is the separation between A_1 and A_2, and l_2 is the separation between A_3 and the middle point of the line connecting A_1 and A_2.

Angles at the Nth sample time can be represented, using Eq. (2) and Eq. (C-1) from Appendix C, as

$$[\alpha_N \ \beta_N] = B\big\{C[D_1 D_2 D_3]\big\}^T \tag{3}$$

where

$$B = \begin{vmatrix} 1/l_1 & -1/l_1 & 0 \\ 0.5/l_2 & 0.5/l_2 & -1/l_2 \end{vmatrix}$$

$$C = \left[1, (N-1)\Delta t, 1/3\Delta t^2, \Delta t^2/6\right], \quad N = 2$$

$$C = \left[1, (N-1)\Delta t, (0.5N - 2/3)\Delta t^2, (N-2)\Delta t^2, \cdots, (N-i)\Delta t^2, \cdots, \Delta t^2, \Delta t^2/6\right],$$

$$N > 2$$

$\Delta t =$ sampling interval

$D_i = [d_{i1} v_{i1} a_{i1} a_{i2}, \cdots, a_{iN}]^T$

$d_{i1} =$ initial position of d_{iN}

$v_{i1} =$ initial velocity of d_{iN}

$d_{iN} =$ displacement estimation at the Nth sample time from a_i's

$a_{i1}\, a_{i2}, \cdots, a_{iN} =$ accelerometer outputs from accelerometer $A_i, i = 1, 2, 3$

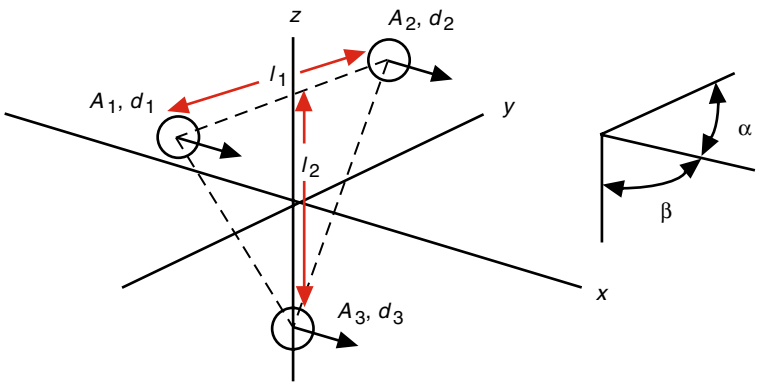

Fig. 2. Triangular configuration of three accelerometers.

B. Algorithm Description

Figure 3 shows all the major signal flows, from three accelerometer measurements, two angle reference inputs (beacon centroids), and the final outputs of the two angular position estimates of the APEA. Additional inputs are reference signals in terms of beacon centroids (x-axis, y-axis). The linear displacement estimator produces three displacement estimates corresponding to the three accelerometer outputs. Combined with the three initial positions derived from the beacon centroids, three position estimates (p_1, p_2, p_3) are obtained. These are, in turn, inputs to the initial velocity and acceleration bias estimator. The details of the initial velocity and acceleration bias estimation using the least-squares method are described in Appendix B. The estimated initial velocity and acceleration bias are fedback to the linear displacement estimator to improve the next position estimations. The final angular position estimations

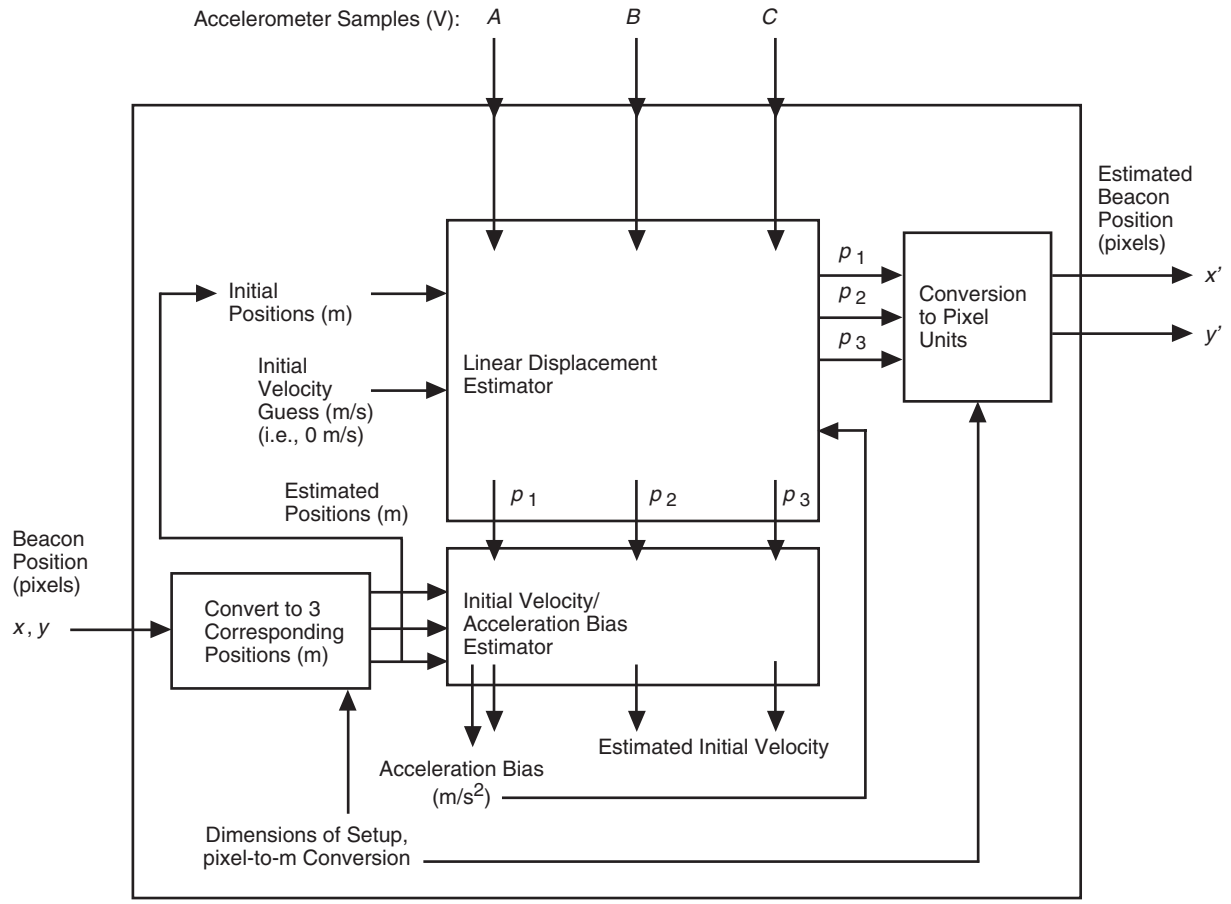

Fig. 3. APEA block diagram showing major signal flows.

are obtained from the estimated three linear positions, after performing the linear displacement-to-angle conversion [Eq. (2)]. The rate of celestial reference inputs to the APEA determines the reference reset period, N. For example, if $N = 2$, every second beacon position output is an estimation while the other is the true beacon position. If $N = 5$, every 5th output is the true beacon position. For this experiment, we did not do any smoothing over multiple beacon samples due to the noise of the accelerometers.

III. Simulation Results

The three-accelerometer configuration of the experimental setup that was used for the simulation is shown in Fig. 4. Sinusoidal signals of 1, 10, and 100 Hz for vibration were used with an assumption of zero measurement noise. The only error sources are the algorithm errors of the APEA. Figures 5 and 6 show the displacement estimation results. As shown, the error increases with both the frequency of the vibration signal and the reference reset period.

IV. Experimental Results

For the experiment, three accelerometers were mounted around the optical communications terminal, and the entire setup was placed on the vibration table (Fig. 7). The experimental procedure is as follows.

(1) Generate the angular spacecraft vibration signal to command the piezo-actuator. In this experiment, the laboratory-measured Cassini spacecraft vibration [linear acceleration power spectral density (PSD)] was used to derive the angular vibration signal for a more realistic frequency content of the expected deep-space vibration signal. The amplitude of the vibration signal is inversely proportional to the length of the interface plate of the optical communications terminal. For this experiment, 15 cm was used. The transformation of linear acceleration into rotational displacements was done following the procedure in [9].

(2) Command the piezo-actuator to shake the platform vibration table with derived PSD.

(3) Measure the angular motion (reference vibration signal or beacon centroids) using the optical communications terminal.

(4) Run the angular position estimation algorithm with various reference reset periods.

(5) Compute the angular position estimation error.

The derived vibration signal was sampled with a CCD at a 625-Hz rate. The experiment was done for reference reset periods of 2, 3, 5, 7, 9, and 11. The beacon position estimation results are given in Fig. 8. As was indicated in the simulation results, the error is proportional to the frequencies of the vibration signals. The error also grows for larger reference reset periods (Fig. 9).

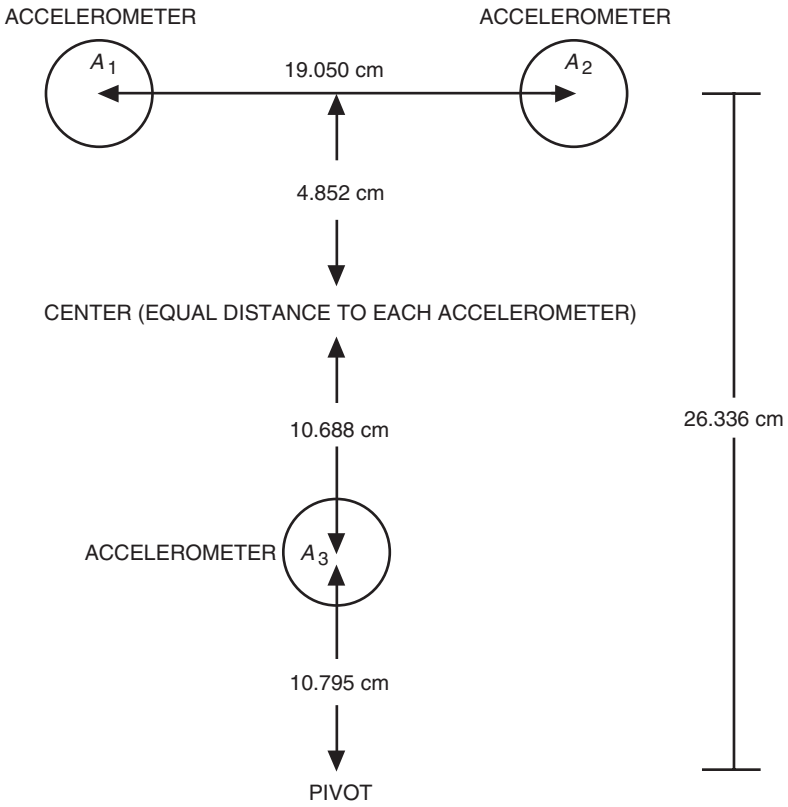

Fig. 4. Dimensions of the separations between three accelerometers, mounted on the optical communications terminal shown in Fig. 7 for the experimental setup.

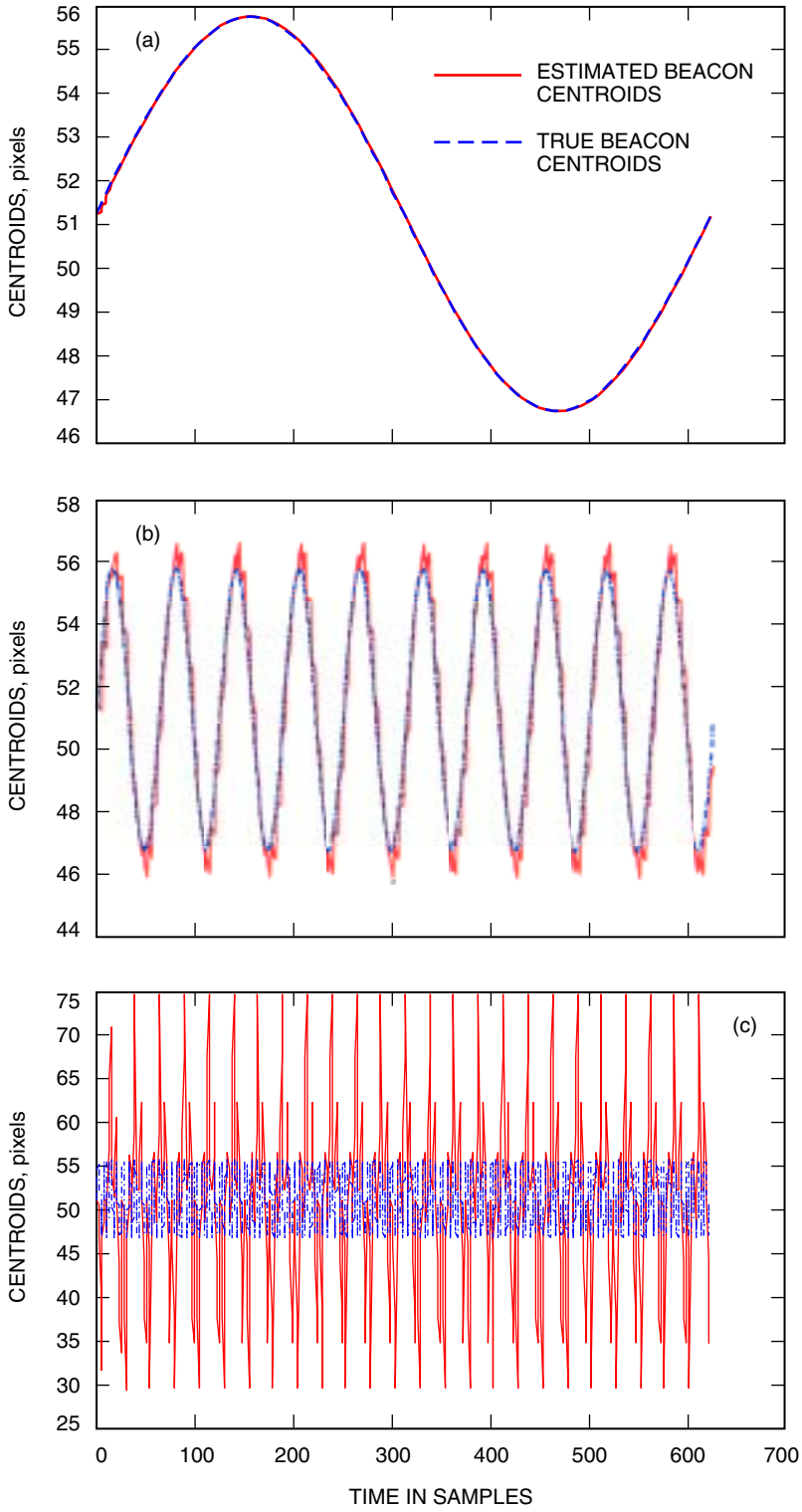

Fig. 5. Simulation results for the reference period of 5: (a) 1-Hz sine wave, (b) 10-Hz sine wave, and (c) 100-Hz sine wave. The estimation error increases with the frequencies of the vibration signals.

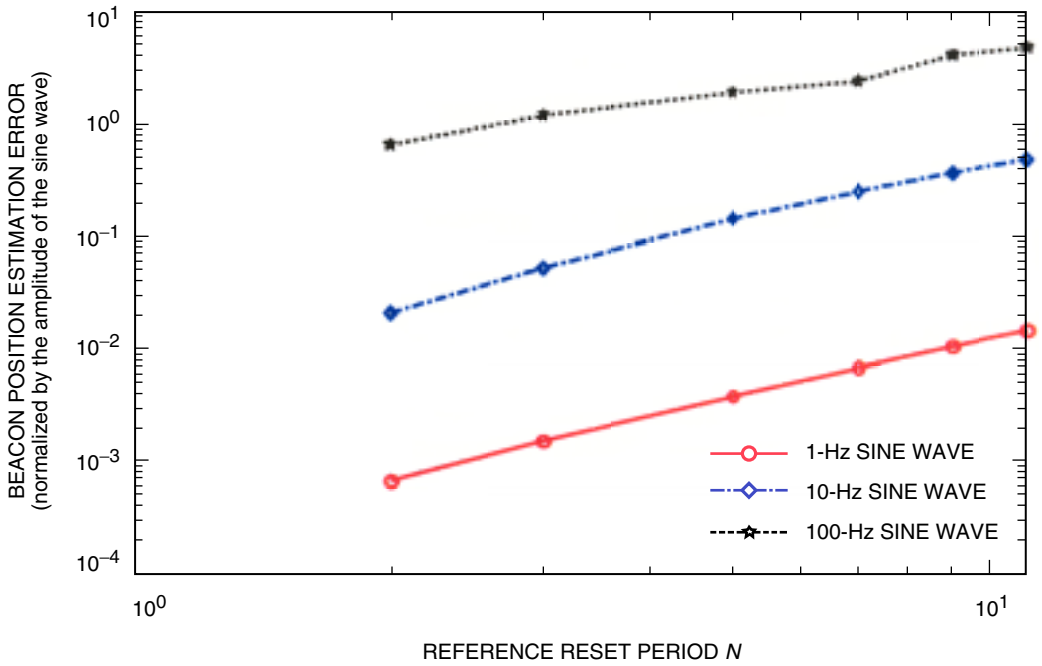

Fig. 6. Angular position estimation error as a function of reference reset periods for sinusoidal signals of 1, 10, and 100 Hz. The error is proportional to both the reference reset period and frequencies of the underlying vibration signals.

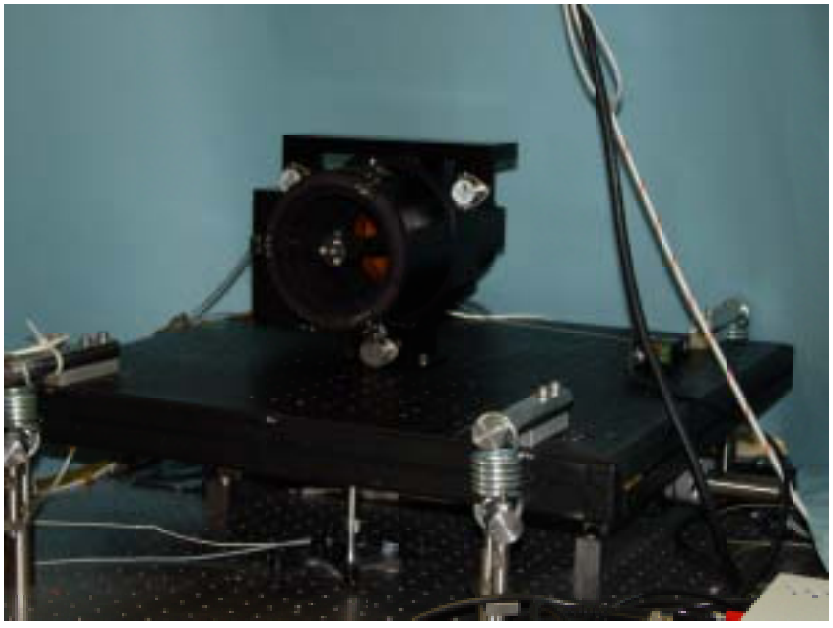

Fig. 7. The experimental setup. Three accelerometers were mounted around the optical communications terminal, and the entire terminal was placed on the vibration table. The piezo-actuator underneath was commanded to shake the vibration table with the generated vibration signal.

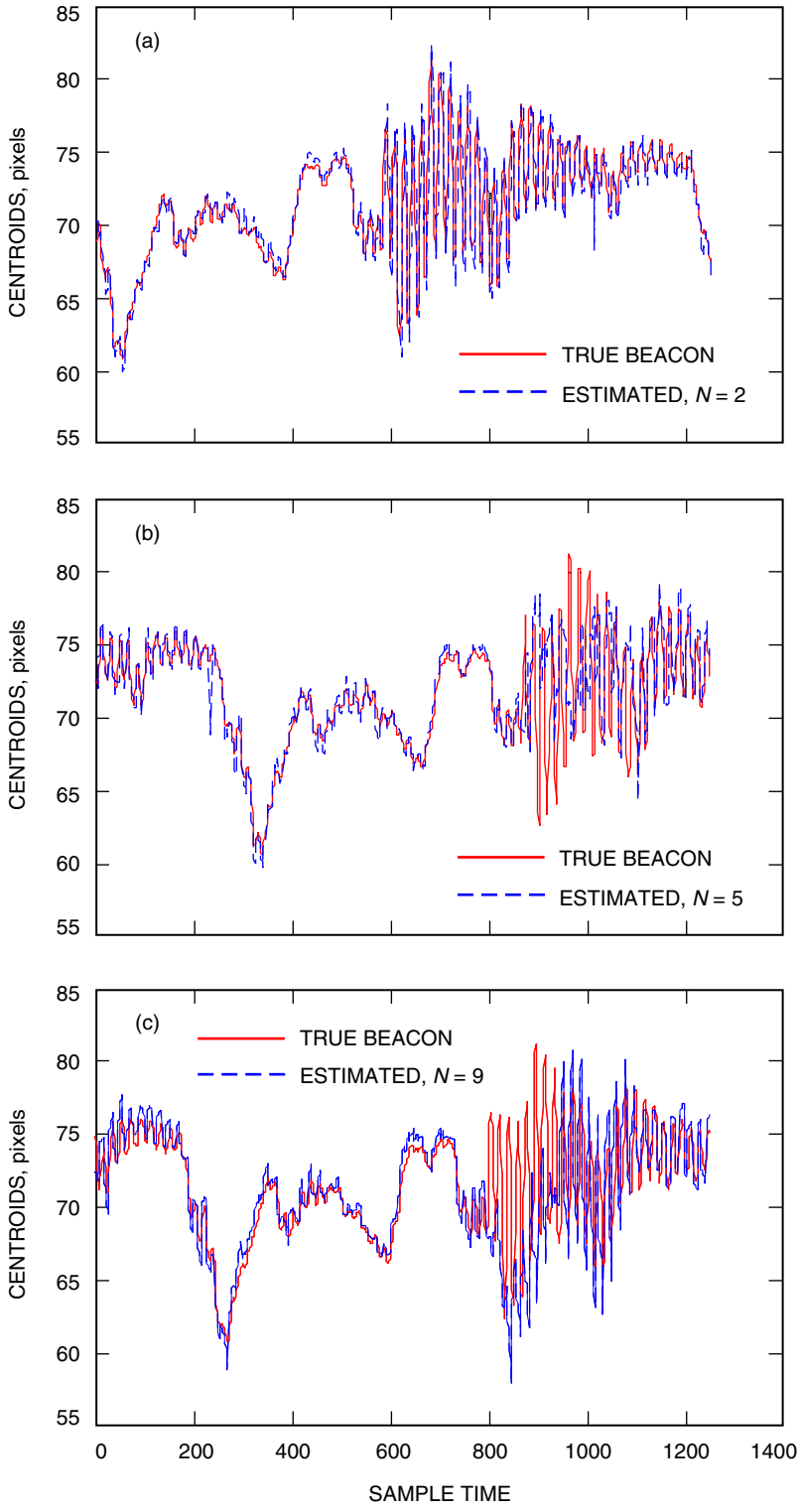

Fig. 8. Experimental results for reference periods of (a) 2, (b) 5, and (c) 9. As was shown in the simulation results, the larger error is noticeable for larger reset periods.

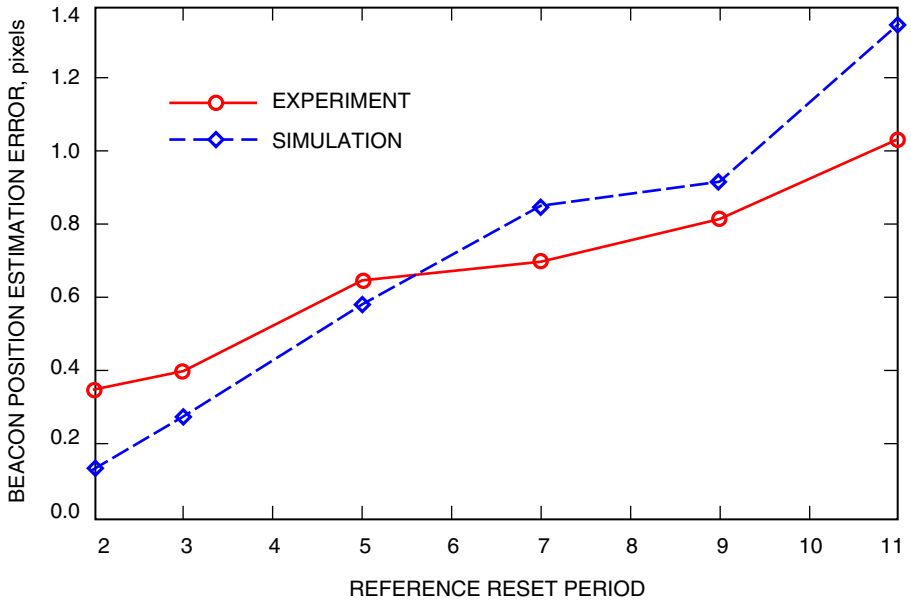

Fig. 9. Comparison of the experimental result with the simulation result. The measured vibration on the CCD of the optical communications terminal was used for the simulation with an assumption of zero noise in the acceleration data. Overall estimation (rms) errors match between the two results; however, the reason why the experimental result is better than the simulation after a reference reset period of 5 requires further analysis.

V. Discussion

Overall, the simulation and experimental results matched closely. The better results of the simulation than those of the experiment after the reference reset period of 5 are somewhat unexpected and need further analysis to explain. The amplitude of the vibration signal shown in Fig. 8 is about ±10 pixels (or 36.1 μrad). The resulting angular position error is about 1 pixel (or 3.61 μrad) for the reference reset period of 11 (Fig. 9). Since the estimation error is directly proportional to the amplitude of the vibration signal, the desired submicroradian pointing is achievable for the deep-space optical communications if the spacecraft vibration can be suppressed below a certain threshold. The threshold depends on the amplitude and frequency contents of the specific spacecraft vibration. For our experiment, about one-third of the given vibration amplitude, or ±12 μrad, would give microradian-level error in angular position estimation for the reference reset period of 11, as an example. This would increase beacon tracking bandwidth by 11 times. Therefore, tracking bandwidth of 1 kHz can be achieved with a beacon tracking rate of 91 Hz. In terms of platform vibration in deep space, the question whether the vibration signal used for our experiment represents the deep-space spacecraft needs to be answered in the future since there are no measured deep-space data currently available to compare. Given the fact that the used angular vibration signal is similar to that of the OLYMPUS spacecraft (a large Earth-orbiting satellite with solar arrays, launched in 1994), we believe that lower vibration is achievable for the deep-space spacecraft with much improved vibration-isolation technologies.

VI. Summary

We have presented an angular position estimation algorithm with error analysis, simulation, and experimental results. The concept of using linear accelerometers to increase the tracking bandwidth can be applied for deep-space optical communications tracking and pointing with a trade-off for the additional error in the beacon position estimations. Our simulation and experimental results showed good agreement

in the beacon position estimations with the various reference reset periods. The results also showed that the estimation error is proportional to both the reference reset period and the frequencies of the vibration signals.

References

[1] H.-H. Chen, S.-C. Lee, and D. D. DeBra, "Gyroscope Free Strapdown Inertial Measurement Unit by Six Linear Accelerometers," *Journal of Guidance, Control, and Dynamics,* vol. 17, pp. 286–290, 1994.

[2] J. W. Alexander, S. Lee, and C.-C. Chen, "Pointing and Tracking Concepts for Deep-Space Missions," *Free-Space Laser Communication Technologies XI, Proceedings of the SPIE,* vol. 3615, pp. 230–249, 1999.

[3] M. C. Algrain and J. Quinn, "Accelerometer Based Line-of-Sight Stabilization Approach for Pointing and Tracking Systems," Second IEEE Conference on Control Applications, Vancouver, British Columbia, Canada, pp. 159–163, September 1993.

[4] M. Kayton and W. R. Fried, *Avionics Navigation Systems,* New York: John Wiley & Sons, Inc., 1997.

[5] J. G. T. Ribeiro, J. T. P. Castro, and J. L. F. Freire, "Problems in Analogue Double Integration to Determine Displacements from Acceleration Data," *Proceedings of the 15th International Modal Analysis Conference,* Orlando, Florida, pp. 930–934, 1997.

[6] J. G. T. Ribeiro, J. J. F. Freire, and J. T. P. Castro, "Some Comments on Digital Integration to Measure Displacements Using Accelerometers," *Proceedings of the 17th International Modal Analysis Conference,* Orlando, Florida, pp. 554–559, 1999.

[7] T. Tolker-Nielsen and G. Oppenhauser, "In-Orbit Result of an Operational Optical Intersatellite Link between ARTEMIS and SPOT4, SILEX," *Free-Space Laser Communication Technologies XIV, Proceedings of the SPIE,* vol. 4635, pp. 1–15, 2002.

[8] The Hubble telescope pointing control system, http://hubble.nasa.gov/technology/pointing-system.html

[9] M. Wittig, L. Van Holtz, D. E. L. Tunbridge, and H. C. Vermeulen, "In-Orbit Measurements of Microaccelerations of ESA's Communication Satellite OLYMPUS," *Free-Space Laser Communication Technologies II, Proceedings of the SPIE,* vol. 1218, pp. 205–214, 1990.

Appendix A

Linear Displacement Estimation—Double Integration Using the Trapezoidal Method

We assume that the spacecraft experiences the continuous acceleration represented as an acceleration function ($a(t)$). The $a(t)$ is sampled at a fixed rate, producing the samples denoted as a_N for its Nth sample, taken at time T_N. The acceleration sample is assumed to require no integration time. The corresponding estimates for velocity and position are denoted by v_N and p_N, respectively.

Let $a_N(t)$ represent continuous acceleration between sampled accelerations a_N and a_{N+1}, where $t = 0$ corresponds to the sampling time T_N. Since there is no further information available between the two samples, we assume the intermediate acceleration value varies linearly. We introduce the linear interpolation function $a_N(t)$ with a sampling interval of $[0, \Delta t]$ defined by

$$a_N(t) = \frac{(a_{N+1} - a_N)t}{\Delta t} + a_N \tag{A-1}$$

Note that, for $t = \Delta t$,

$$a_N(\Delta t) = a_{N+1} \tag{A-2}$$

Let's consider only two sample points, a_N and a_{N+1}. The integration of $a_N(t)$ from 0 to t gives the corresponding velocity, $v_N(t)$:

$$v_N(t) = \frac{(a_{N+1} - a_N)t^2}{2\Delta t} + a_N t + v_N, \quad v_N \text{ initial velocity at } t = 0 \tag{A-3}$$

For $t = \Delta t$,

$$v_N(t = \Delta t) = v_{N+1} = \frac{(a_{N+1} + a_N)\Delta t}{2} + v_N \tag{A-4}$$

which is the area below the straight line connecting the two points a_N and a_{N+1} in Fig. A-1. Notice that the error exists in the velocity estimate due to the difference between the true area and our estimate because of our assumption on linearly varying acceleration. This velocity error propagates through position estimates.

Similarly, for the position estimate, integrating Eq. (A-3) gives

$$p_N(t) = \frac{(a_{N+1} - a_N)t^3}{6\Delta t} + a_N \frac{t^2}{2} + v_N t + p_N, \quad p_N \text{ position at } t = 0 \tag{A-5}$$

For $t = \Delta t$,

$$p_N(t=\Delta t) = p_{N+1} = (a_{N+1} - a_N)\frac{\Delta t^2}{6} + a_N\frac{\Delta t^2}{2} + v_N\Delta t + p_N$$

$$= a_{N+1}\frac{\Delta t^2}{6} + a_N\frac{\Delta t^2}{3} + v_N\Delta t + p_N \qquad \text{(A-6)}$$

The procedure in Eq. (A-6) is summarized in Fig. A-2.

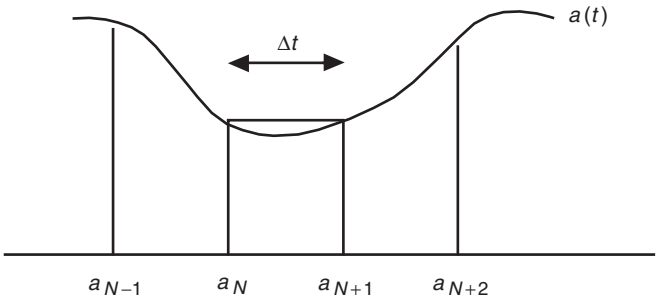

Fig. A-1. A sampling of continuous acceleration $a(t)$.

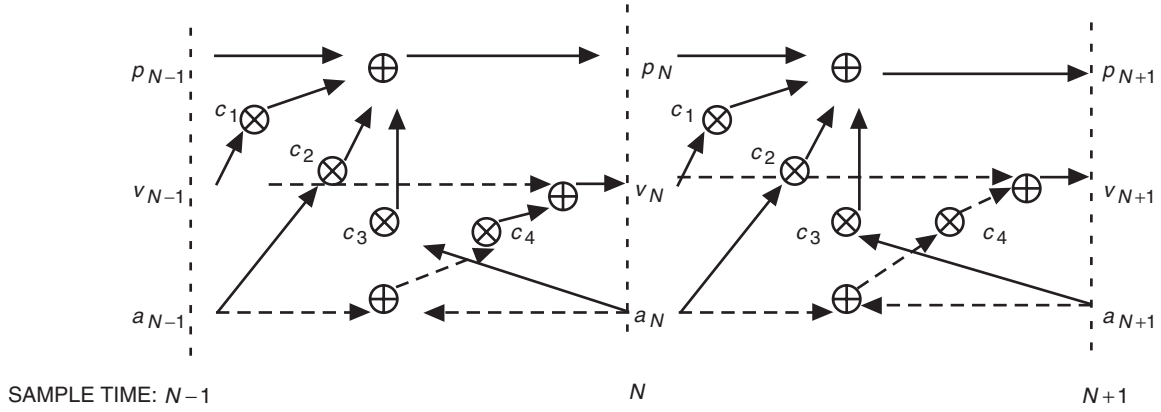

Fig. A-2. The position estimation procedure from acceleration measurements. The multipliers (c_1 to c_4) are $c_1 = \Delta t$, $c_2 = \Delta t^2/3$, $c_3 = \Delta t^2/6$, and $c_4 = \Delta t/2$.

Appendix B

Initial Velocity and Acceleration Bias Estimation Using the Least-Squares Method

As was shown in Eq. (A-6), initial velocity needs to be estimated for accurate displacement estimation. Also, acceleration bias needs to be estimated and corrected due to the possibility of any misalignment of accelerometers with respect to a reference direction.

Let

$v_0 =$ initial velocity

$a_b =$ acceleration bias

$B_n =$ beacon measurements

$P_n =$ estimated displacement from acceleration, a_n for $n = 1, 1+M, 1+2M, \cdots$ (M = intervals for evaluation)

Since P_n is a function of sampling time, t_n, and acceleration, a_n, the displacement estimation error, E_n, can be written as

$$E_n = P_n + \frac{a_b(n\Delta t)^2}{2} + v_0 n\Delta t - B_n \tag{B-1}$$

where Δt is the sampling interval. Let the error function to be minimized be

$$S = \sum_n E_n^2, \quad \text{for } n = M, 2M, \cdots \tag{B-2}$$

Minimizing by

$$\left.\begin{aligned} \frac{dS}{da_b} &= 0 \\ \frac{dS}{dv_0} &= 0 \end{aligned}\right\} \tag{B-3}$$

gives

$$\sum_n \left(a_b n^4 \frac{\Delta t^2}{2} + v_0 n^3 \Delta t \right) = \sum_n (B_n - P_n) n^2 \tag{B-4}$$

$$\sum_n \left(a_b n^3 \frac{\Delta t^2}{2} + v_0 n^2 \Delta t \right) = \sum_n (B_n - P_n) n \tag{B-5}$$

where $n = M, 2M, \cdots$.

From Eqs. (B-4) and (B-5),

$$a_b = \frac{\begin{bmatrix} \sum(B_n - P_n)n^2 & \sum n^3 \Delta t \\ \sum(B_n - P_n)n & \sum n^2 \Delta t \end{bmatrix}}{\begin{bmatrix} \sum n^4 \Delta t^2/2 & \sum n^3 \Delta t \\ \sum n^3 \Delta t^2/2 & \sum n^2 \Delta t \end{bmatrix}} \tag{B-6}$$

$$v_0 = \frac{\begin{bmatrix} \sum n^4 \Delta t^2/2 & \sum(B_n - P_n)n^2 \\ \sum n^3 \Delta t^2/2 & \sum(B_n - P_n)n \end{bmatrix}}{\begin{bmatrix} \sum n^4 \Delta t^2/2 & \sum n^3 \Delta t \\ \sum n^3 \Delta t^2/2 & \sum n^2 \Delta t \end{bmatrix}} \tag{B-7}$$

The implementation of Eqs. (B-6) and (B-7) requires minimum intervals of two for two variables, a_b and v_0. Figure B-1 illustrates an example for the two-interval case.

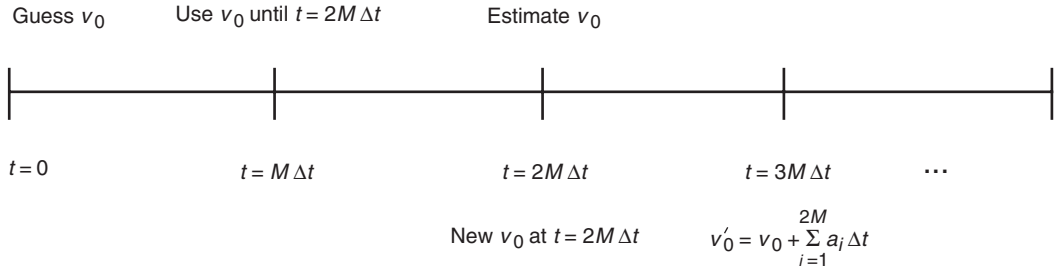

Fig. B-1. An example of the two-interval case for acceleration bias and initial velocity estimation.

Appendix C
Error Analysis

In this appendix, random error caused by the noise in the acceleration measurements is investigated. The measurement noise includes accelerometer electronic noise, quantization (analog-to-digital) noise, amplifier noise, radiation noise, etc.

In order to express the relationship between random error and position estimation error, Eq. (A-6) needs to be rewritten in terms of acceleration with initial values of velocity and position. From Eq. (A-6),

$$
\left.
\begin{aligned}
p_1, v_1 &= \text{initial values of position and velocity} \\
p_2 &= a_2\frac{\Delta t^2}{6} + a_1\frac{\Delta t^2}{3} + v_1\Delta t + p_1 \\
p_3 &= a_3\frac{\Delta t^2}{6} + a_2\frac{\Delta t^2}{3} + v_2\Delta t + p_2 \\
&= a_3\frac{\Delta t^2}{6} + a_2\frac{\Delta t^2}{3} + a_2\frac{\Delta t^2}{6} + a_1\frac{\Delta t^2}{3} + (a_2+a_1)\frac{\Delta t^2}{2} + 2v_1\Delta t + p_1 \\
p_4 &= a_4\frac{\Delta t^2}{6} + a_3\frac{\Delta t^2}{3} + v_3\Delta t + p_3 \\
&= a_4\frac{\Delta t^2}{6} + a_3\frac{\Delta t^2}{3} + a_3\frac{\Delta t^2}{6} + a_2\frac{\Delta t^2}{3} + (a_3+a_2)\frac{\Delta t^2}{2} \\
&\quad + a_2\frac{\Delta t^2}{6} + a_1\frac{\Delta t^2}{3} + (a_2+a_1)\frac{\Delta t^2}{2} + (a_2+a_1)\frac{\Delta t^2}{2} + 3v_1\Delta t + p_1 \\
&\vdots \\
p_N &= \Delta t^2\frac{(a_2+\cdots+a_N)}{6} + \Delta t^2\frac{(a_1+\cdots+a_{N-1})}{3} + (N-1)v_1\Delta t + p_1 \\
&\quad + (N-2)a_1\frac{\Delta t^2}{2} + (2N-5)a_2\frac{\Delta t^2}{2} + (2N-7)a_3\frac{\Delta t^2}{2} \\
&\quad + (2N-9)a_4\frac{\Delta t2}{2} + \cdots \\
&= \sum_{i=2}^{N-1}(N-i)a_i\Delta t^2 + \left(\frac{N}{2} - \frac{2}{3}\right)a_1\Delta t^2 + a_N\frac{\Delta t^2}{6} + (N-1)v_1\Delta t + p_1
\end{aligned}
\right\} \quad \text{(C-1)}
$$

where N is the number of acceleration measurements and Δt is the sampling period such that $N = T/\Delta t$ for the total integration time of T.

As shown in Eq. (C-1), the knowledge of initial velocity, v_1, plays an important role in estimating the position. The equation indicates that the position estimation error is proportional to the error in initial velocity and the integration period. Since the accelerometer does not provide initial velocity information, the initial velocity must be obtained either from direct measurements using lower bandwidth rate sensors such as gyros or from estimations using optical measurements of the beacon data. The effect of any error in initial velocity estimation will become larger as the integration period increases. The same is true for any acceleration bias present in acceleration measurements, which alters velocity. In this article, we have assumed that there is no accelerometer bias and that the initial velocity is known. Estimation of acceleration bias and initial velocity will be addressed in a future article, along with implementation progress.

The position estimation error (variance) can be expressed as a function of the random error (1 sigma value) in acceleration, σ_a, assuming the a_i's are independent, identically distributed (i.i.d.) random variables:

$$\sigma_{pN}^2 = (\Delta t^2)^2 \sum_{i=2}^{N-1} (N-i)^2 \sigma_a^2 + (\Delta t^2)^2 \left(\frac{N}{2} - \frac{2}{3}\right)^2 \sigma_a^2 + \sigma_a^2 \frac{(\Delta t^2)^2}{6^2}$$

The standard deviation of position estimation using N samples of acceleration measurements then becomes

$$\sigma_{pN} = \Delta t^2 \sigma_a \left(\sum_{i=2}^{N-1} (N-i)^2 + \left(\frac{N}{2} - \frac{2}{3}\right)^2 + \frac{1}{36} \right)^{1/2} \tag{C-2}$$

An angular position estimation error can be derived from Eq. (C-1) assuming the two linear position estimates, d_1 and d_2, are i.i.d. random variables with an rms error of σ_{pN} in Eq. (C-2):

$$\sigma_\theta^2 = \frac{\mathrm{Var}(d_1) + \mathrm{Var}(d_2)}{l_2}$$

$$= \frac{2\sigma_{pN}^2}{l_2} \tag{C-3a}$$

or

$$\sigma_\theta = \frac{\sqrt{2}\sigma_{pN}}{l} \tag{C-3b}$$

Equations (C-2) and (C-3) imply that the random error is proportional to the acceleration measurement's noise and the integration period, N. However, it is inversely proportional to sampling rate ($1/\Delta t$) and the separation between the accelerometers.